

A simple tensor network algorithm for two-dimensional steady states

Augustine Kshetrimayum,¹ Hendrik Weimer,² and Román Orús^{1,*}

¹*Institute of Physics, Johannes Gutenberg University, 55099 Mainz, Germany*

²*Institut für Theoretische Physik, Leibniz Universität Hannover, Appelstr. 2, 30167 Hannover, Germany*

Understanding dissipation in 2D quantum many-body systems is a remarkably difficult open challenge. Here we show how numerical simulations for this problem are possible by means of a tensor network algorithm that approximates steady states of 2D quantum lattice dissipative systems in the thermodynamic limit. Our method is based on the intuition that strong dissipation kills quantum entanglement before it gets too large to handle. We test its validity by simulating a dissipative quantum Ising model, relevant for dissipative systems of interacting Rydberg atoms, and benchmark our simulations with a variational algorithm based on product and correlated states. Our results support the existence of a first order transition in this model, with no bistable region. We also simulate a dissipative spin-1/2 XYZ model, showing that there is no re-entrance of the ferromagnetic phase. Our method enables the computation of steady states in 2D quantum lattice systems.

INTRODUCTION

Understanding the effects of dissipation in quantum many-body systems is an open challenge. When the quantum system is immersed in an environment and coupled to it, the exchange of information (e.g., energy, heat, particles) between system and environment usually leads to dissipation when the environment is larger than the system. If the dissipation is Markovian (i.e., if no information flows back into the system), then the evolution is generated by a Liouvillian superoperator \mathcal{L} , and can be casted in the form of a master equation for the reduced density matrix of the quantum system. As time flows, the system dissipates, until reaching in many cases a steady, or “dark” state ρ_s , so that $\mathcal{L}[\rho_s] = 0$. This process is important in several contexts, e.g., understanding the decoherence of complex wavefunctions [1], quantum thermodynamics [2], engineering of topological order through dissipation [3], and driven-dissipative universal quantum computation [4]. The study of non-equilibrium quantum complex systems has recently received much attention [5–9].

In this paper we present a method to approximate such steady states for 2D quantum lattice systems of infinite size (i.e., in the thermodynamic limit). Over the years, the solution to this problem has been shown to be remarkably difficult. Our method is to be compared to alternatives in 2D such as cluster mean-field methods [10], correlated and product state variational ansatz [11, 12], and corner-space renormalization group [13]. Importantly, none of these methods targets the truly 2D quantum correlations that are present in the problem. The method that we propose here is based on tensor networks (TN) [14–18] and is, in fact, particularly simple and efficient. Whereas TN methods have been used in the context of dissipative 1D systems [19–21] and thermal 2D states [22, 23], our method uses truly 2D TNs to target 2D dissipation. To show the validity of our algorithm, we compute the steady states of the dissipa-

tive 2D quantum Ising model for spin-1/2, which is of relevance for controversies concerning dissipation for interacting Rydberg atoms [11]. As we shall discuss, we compare our results with those obtained by a variational algorithm based on product and correlated states [12]. Moreover, we also simulate a dissipative spin-1/2 XYZ model, showing that there is no re-entrance of the ferromagnetic phase, compatible with recent cluster mean-field results [10].

RESULTS

Parallelism with imaginary-time evolution

We start by considering a master equation of the form

$$\dot{\rho} = \mathcal{L}[\rho] = -i[H, \rho] + \sum_{\mu} \left(L_{\mu} \rho L_{\mu}^{\dagger} - \frac{1}{2} \{L_{\mu}^{\dagger} L_{\mu}, \rho\} \right), \quad (1)$$

where ρ is the density matrix of the system, \mathcal{L} is the Liouvillian superoperator, H the Hamiltonian of the system, and $\{L_{\mu}, L_{\mu}^{\dagger}\}$ the Lindblad operators responsible for the dissipation. Following a similar approach as in Ref. [24], we can also write the same equation in vectorized form using the so-called “Choi’s isomorphism”, i.e., understanding the coefficients of ρ as those of a vector $|\rho\rangle_{\sharp}$ (intuitively, $|a\rangle\langle b| \simeq |a\rangle \otimes |b\rangle$, see Fig. 1(a)): $|\dot{\rho}\rangle_{\sharp} = \mathcal{L}_{\sharp} |\rho\rangle_{\sharp}$, where the “vectorized” Liouvillian is given by

$$\mathcal{L}_{\sharp} \equiv -i(H \otimes \mathbb{I} - \mathbb{I} \otimes H^T) + \sum_{\mu} \left(L_{\mu} \otimes L_{\mu}^* - \frac{1}{2} L_{\mu}^{\dagger} L_{\mu} \otimes \mathbb{I} - \frac{1}{2} \mathbb{I} \otimes L_{\mu}^* L_{\mu}^T \right). \quad (2)$$

In the above equation, the symbol of tensor product \otimes separates operators acting on either the l.h.s. (ket) or the r.h.s. (bra) of ρ in its matrix form. Whenever \mathcal{L}_{\sharp} is independent of time, time evolution can be formally written as $|\rho(T)\rangle_{\sharp} = e^{T\mathcal{L}_{\sharp}} |\rho(0)\rangle_{\sharp}$, which for very large

times T may yield a steady state $|\rho_s\rangle_{\#} \equiv \lim_{T \rightarrow \infty} |\rho(T)\rangle_{\#}$. It is easy to see that the state $|\rho_s\rangle_{\#}$ is the eigenvector of \mathcal{L} corresponding to zero eigenvalue, so that $\mathcal{L}_{\#}|\rho_s\rangle_{\#} = 0$.

Next, let us consider the special but quite common case in which the Liouvillian \mathcal{L} can be decomposed as a sum of local operators. For nearest-neighbor terms, one has the generic form $\mathcal{L}[\rho] = \sum_{\langle i,j \rangle} \mathcal{L}^{[i,j]}[\rho]$, where the sum $\langle i,j \rangle$ runs over nearest-neighbors. In the “vectorized” notation ($\#$), this means that $\mathcal{L}_{\#} = \sum_{\langle i,j \rangle} \mathcal{L}_{\#}^{[i,j]}$.

The combination of the expressions above yields a parallelism with the calculation of ground states of local Hamiltonians by imaginary-time evolution, which we detail in Table I.

Ground states	Steady states
$H = \sum_{\langle i,j \rangle} h^{[i,j]}$	$\mathcal{L}_{\#} = \sum_{\langle i,j \rangle} \mathcal{L}_{\#}^{[i,j]}$
$e^{-\tau H}$	$e^{T \mathcal{L}_{\#}}$
$ e_0\rangle$	$ \rho_s\rangle_{\#}$
$\langle e_0 H e_0 \rangle = e_0$	$\# \langle \rho_s \mathcal{L}_{\#} \rho_s \rangle_{\#} = 0$
Imaginary time τ	Real time T

TABLE I: Parallelism between the calculation of ground states by imaginary-time evolution, and the calculation of steady states by real-time evolution. On the left hand side, H is a Hamiltonian that decomposes as a sum of local terms $h^{[i,j]}$, $|e_0\rangle$ is the ground state of H with eigenvalue e_0 , and τ is the imaginary time.

Computing 2D steady states

Given the parallelism above, it is clear that one can adapt, at least in principle, the methods to compute imaginary time evolution of a pure state as generated by local Hamiltonians, to compute also the real time evolution of a mixed state as generated by local Liouvillians. This was, in fact, the approach taken in Ref. [24] for finite-size 1D systems, using Matrix Product Operators (MPO) [25] to describe the 1D reduced density matrix, and proceeding as in the Time-Evolving Block Decimation (TEBD) algorithm for ground states of 1D local Hamiltonians [26, 27].

Inspired by the above parallelism, our method for 2D systems proceeds by representing the reduced density operator ρ by a Projected Entangled-Pair Operator (PEPO) [14–18] with physical dimension d and bond dimension D , see Fig. 1(b). Such a construction does not guarantee the positivity of the reduced density matrix [28]. However, we shall see later that this lack of exact positivity is not too problematic in our numerical simulations. Once vectorized, the PEPO can be understood as a Projected Entangled Pair State (PEPS) [29] of physical dimension d^2 and bond dimension D , as shown also in Fig. 1(b). Next, we notice that for the case of an infinite-size 2D system, this setting is actually equivalent

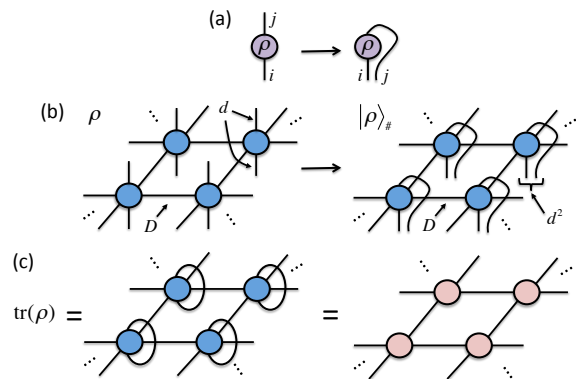


FIG. 1: **Relevant tensor network diagrams.** (a) Tensor network diagram for the reduced density matrix ρ , with matrix elements ρ_i^j . The vectorization is, simply, reshaping the two indices into a single one; (b) tensor network diagram for the PEPO of ρ on a 2D square lattice, with bond dimension D and physical dimension d . When vectorized, it can be understood as a PEPS for $|\rho\rangle_{\#}$ with physical dimension d^2 ; (c) The trace of ρ maps to the contraction of a 2D network of tensors.

to that of the infinite-PEPS algorithm (iPEPS) to compute ground states of local Hamiltonians in 2D in the thermodynamic limit [30]. Thus, in principle, we can use the full machinery of iPEPS to tackle as well the problem of 2D dissipation and steady states.

There seems to be, however, one problem with this idea: unlike in imaginary-time evolution, we are now dealing with real time. In the master equation, part of the evolution is generated by a Hamiltonian H , and part by the Lindblad operators L_{μ} . The Hamiltonian part corresponds actually to a unitary “Schrodinger-like” evolution in real time, which typically increases the “operator-entanglement” in $|\rho\rangle_{\#}$, up to a point where it may be too large to handle for a TN representation (e.g., 1D MPO or 2D PEPO) with a reasonable bond dimension. In 1D this is the reason why the simulations of master equations are only valid for a finite amount of time. In 2D, simple numerical experiments indicate that in a typical simulation the growth of entanglement is even faster than in 1D.

Luckily, this is not a dead-end: if the dissipation is strong compared to the rate of entanglement growth, then the evolution drives the system into the steady state before hitting a large-entanglement region. The main point of this paper is to show that this is indeed the case for 2D dissipative systems. Regarding settings where dissipation is not so strong, our algorithm is a good starting point to compute steady states in the strong-dissipation regime. The strength of the dissipation can then be lowered down adiabatically, and using as initial state the one pre-computed for slightly-stronger dissipation. In this way one may get rid of local minima and obtain good results also in the weak dissipation regime.

With this in mind, our algorithm just applies the

iPEPS machinery to compute the time evolution in 2D with a local Liouvillian \mathcal{L} and some initial state. For the examples shown in this paper, we use the so-called simple update scheme [31] for the time-evolution of the PEPO, Corner Transfer Matrices (CTM) [32–39] for the calculation of observables (other approaches [40–49] would also be equally valid here), and random initial states. To check whether we have a good approximation of a steady state or not we compute the parameter $\Delta \equiv \text{tr}[\rho_s \mathcal{L}_\#^\dagger \rho_s]$. For a good steady-state approximation, this parameter should be close enough to zero, since we have $\Delta = 0$ in the exact case (in practice, we saw that the imaginary part of Δ is negligible, $\text{Im}(\Delta) \sim 10^{-15}$. Moreover, it should also be possible to check directly $\text{tr}[\rho_s \mathcal{L}_\#^\dagger \mathcal{L}_\# \rho_s]$, but this is computationally more costly and does not change the conclusions of our observations). Another quantity that we used to check the validity of the simulations is the sum of negative eigenvalues of the (numerical) reduced density matrices of the system. More precisely, we define $\epsilon_n \equiv \sum_{i|\nu_i < 0} \nu_i(\rho_n)$, where ρ_n is the reduced density matrix of n contiguous spins in the steady state and $\nu_i(\rho_n)$ its eigenvalues, with only the negative ones entering the sum. In an exact case, this quantity should be equal to zero. However, the different approximations (operator-entanglement truncations) in the method may produce a small negative part in ρ_s , which can be easily quantified in this way (as a word of caution: notice that Δ and ϵ_n can be used to benchmark our calculations, but they do not characterize the distance to the steady state. Moreover, in principle one could also develop a fully-positive algorithm for ρ_n [8], but at the expense of accuracy and efficiency [28]).

The computational cost of this algorithm is the one of the chosen iPEPS strategy. In our case, we work with a simple update for the evolution with a 2-site unit cell, which has a cost of $O(d^4 D^5 + d^{12} D^3)$, and Trotter time-steps $\delta t = 0.1 - 0.01$. The choice of Trotter steps actually depends on the time scales of the particular problem at hand. For the models considered here, we saw empirically that this choice was a good one. The convergence in the number of steps depends on the gap of the Liouvillian: the closer to a gapless point, the slower the convergence. Empirically we observed that this convergence was quite fast in the gapped phases of the models that we studied. Moreover, the CTM method for expectation values is essentially the one used to approximate classical partition functions on a 2D lattice (see Fig. 1(c)), which has a cost of $O(dD^4 + \chi^2 D^4 + \chi^3 D^3)$, being χ the CTM bond dimension. The overall approach is thus remarkably efficient. To have an idea of how efficient this is, let us imagine the following alternative strategy: we consider the Hermitian and positive semidefinite operator $\mathcal{L}_\#^\dagger \mathcal{L}_\#$, and target $|\rho\rangle_\#$ as its ground state. This ground state could be computed, e.g., by an imaginary time evolution. The problem, however, is that the crossed products in $\mathcal{L}_\#^\dagger \mathcal{L}_\#$

are non-local, and therefore the usual algorithms for time evolution are difficult to implement unless one introduces extra approximations in the range of the crossed terms [50]. Another option is to approximate the ground state variationally, e.g., via the Density Matrix Renormalization Group [51–54] or similar approaches [19, 20] in 1D, or variational PEPS in 2D [29]. In the thermodynamic limit, however, this approach does not look very promising because of the non-locality of $\mathcal{L}_\#^\dagger \mathcal{L}_\#$ mentioned before. In any case, one could always represent this operator as a PEPO (in 2D), which would simplify some of the calculations, but at the cost of introducing a very large bond dimension in the representation of $\mathcal{L}_\#^\dagger \mathcal{L}_\#$. For instance, if a typical PEPO bond dimension for $\mathcal{L}_\#$ is ~ 4 , then for $\mathcal{L}_\#^\dagger \mathcal{L}_\#$ it is ~ 16 , which in 2D implies extremely slow calculations. Another option would be to target the variational minimization of the real part for the expectation value of \mathcal{L} [19, 20]. This option, however, is also dangerous in 2D because of the presence of many local minima. Additionally, the correct norm to perform all these optimizations is the one-norm of $\mathcal{L}(\rho)$ which, in contrast to the more usual 2-norm, is a hard figure of merit to optimize with variational TN methods. The use of real-time evolution is thus a safer choice in the context of the approximation of 2D steady states.

Numerical simulations

We first benchmark our method by simulating a dissipative spin-1/2 quantum Ising model on an infinite 2D square lattice, where dissipation pumps one of the spin states into the other. This model is of interest in the context of recent experiments with ultracold gases of Rydberg atoms [55, 56]. Moreover, the phase diagram of its steady state is still a matter of controversy. Initially, it was predicted that the model exhibits a bistable phase [57, 58], but several numerical and analytical calculations have cast doubts on this claim and predict instead a first order transition. In particular, a variational approach [11, 12] and a Monte Carlo wavefunction approach [21] predict that the bistable phase is replaced by a first order transition, which is also supported by arguments derived from a field-theoretical treatment of related models within the Keldysh formalism [59]. Furthermore, it is an open question whether the model supports an antiferromagnetic phase [11, 12, 57, 60, 61]. The master equation follows the one in Eq. (1), where the Hamiltonian part is given by $H = \frac{V}{4} \sum_{\langle i, j \rangle} \sigma_z^{[i]} \sigma_z^{[j]} + \frac{h_x}{2} \sum_i \sigma_x^{[i]} + \frac{h_z}{2} \sum_i \sigma_z^{[i]}$, with $\sigma_\alpha^{[i]}$ the α -Pauli matrix at site i , V the interaction strength, h_x, h_z the transverse and parallel fields respectively, and where the sum over $\langle i, j \rangle$ runs over nearest neighbors. The dissipative part is given by operators $L_\mu = \sqrt{\gamma} \sigma_-^{[\mu]}$, so that in this particular case μ is a site index, and where σ_- is the usual spin-lowering operator.

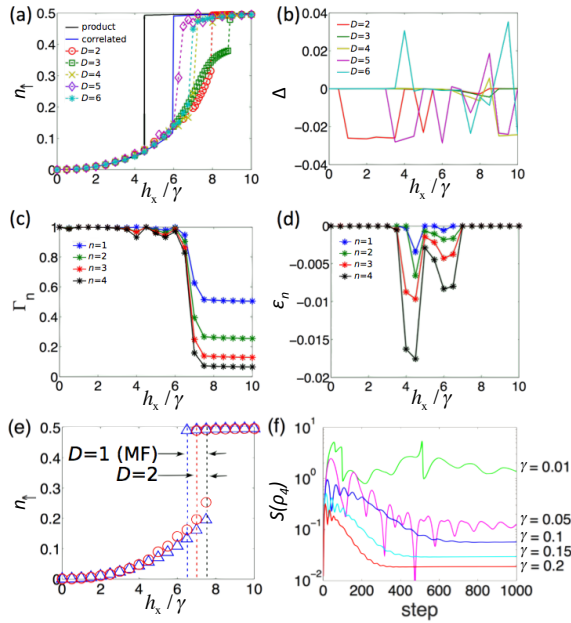


FIG. 2: **Computed quantities.** (a) Spin-up density in the steady state as a function of h_x/γ for $V = 5\gamma$, $\gamma = 0.1$ and $h_z = 0$, as computed with our method up to $D = 6$. For comparison, we show the results obtained by the variational method from Ref.[12] with product states (black line) and correlated states (blue line); (b) Δ up to $D = 6$; (c) Purity Γ_n of the reduced density matrix for a block of n contiguous spins, for $D = 6$ (other bond dimensions have similar behaviour). Spins are chosen within the 2×2 unit cell of the tensor network; (d) ϵ_n of the reduced density matrix for a block of n contiguous spins, for $D = 6$ (other bond dimensions have similar behaviour). Overall, the convergence can be further improved by using more accurate update schemes; (e) bistable region for $D = 1$ (mean field) and $D = 2$. The region shrinks and disappears for larger bond dimension; (f) operator-entanglement entropy throughout the algorithmic evolution for a block a 2×2 unit cell with $D = 2$, $V = 0.5$, $h_x/\gamma = 10$, and different values of γ . The stronger the dissipation, the weaker the entanglement. A similar behaviour is observed for larger D .

In our simulations, we first set $V = 5\gamma$, $\gamma = 0.1$, $h_z = 0$ in order to compare with the results in Ref.[12], which use a correlated variational ansatz with states of the form $\rho = \prod_i \rho_i + \sum_{\langle ij \rangle} C_{ij} \prod_{k \neq ij} \rho_k$, where ρ_i are single site density matrices and C_{ij} account for correlations. We compute the density of spins-up $n_\uparrow \equiv \sum_{i=1}^N \langle (1 + \sigma_z^{[i]}) \rangle / 2N$ (N is the system's size) as a function of h_x/γ , for which it is believed to exist a first order transition in the steady state from a “lattice gas” to a “lattice liquid”. This transition is clearly observed in our simulations in Fig.(2(a)), where simulations for $D = 5, 6$ agree with the correlated variational ansatz in the location of the transition point at $h_x^*/\gamma \sim 6$. In fact, as the bond dimension D increases, we observe that there is more tendency towards agreeing with the correlated variational ansatz. We also observe a non-monotonic convergence in D , which may be due to a stronger effect of the approximations in the transition

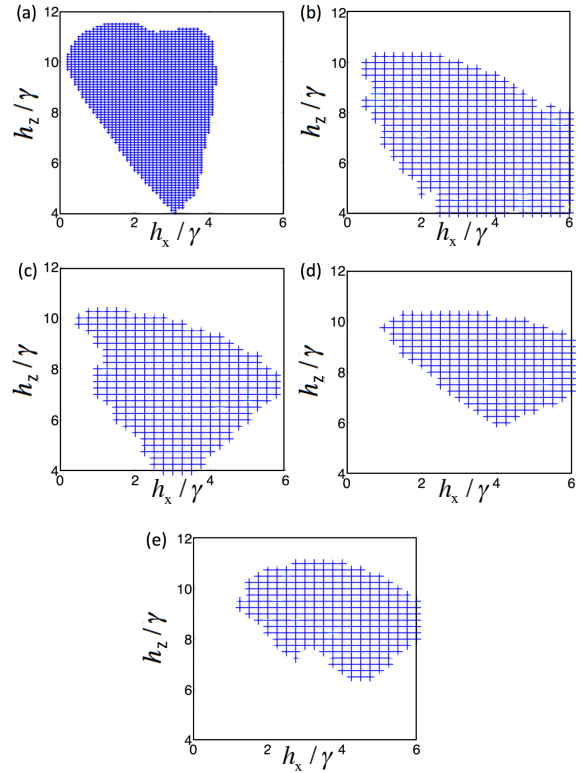


FIG. 3: **Antiferromagnetic region.** In blue, for $V = 5\gamma$ and $\gamma = 0.1$: (a) variational product-state ansatz from Ref.[11]; (b) tensor network method with $D = 2$; (c) $D = 3$; (d) $D = 4$; (e) $D = 5$. We see no antiferromagnetic phase in this region for $D = 6, 7, 8$ and 9 . Numerically, we see that the population difference drops down to $\sim 10^{-9}$ as soon as the antiferromagnetic dissapears, whereas it is $\sim 10^{-1}$ when we observe it.

region, and which remains to be fully understood. Other quantities can also assess this transition, e.g., the purity of the n -site reduced density matrix $\Gamma_n \equiv \text{tr}(\rho_n^2)$, which we plot in Fig.(2(c)) for $D = 6$. We can see from that plot that the steady states ρ_s for low h_x/γ are quite close to a pure state (for which $\Gamma_n = 1/\nu n$). To validate this simulations we computed the parameters Δ and ϵ_n introduced previously, which we show in Fig.(2(b)) and Fig.(2(d)) respectively. One can see that Δ is always quite close to zero in our simulations, being at most $|\Delta| \sim 0.03$, so that the approximated ρ_s is close to the exact steady state. Moreover, one can also see that ϵ_n is always rather small, e.g., for $D = 6$ it is at most $\epsilon_n \sim -0.017$ for the 4-site density matrix close to the transition region (similar conclusions hold for other bond dimensions). This implies that the negative contribution to the numerical reduced density matrix is quite small, and therefore does not lead to large errors. In practice, we see that ϵ_n seems to be extensive in n away from the transition region, more specifically, $\epsilon_n \sim n\epsilon_0 + O(1/n)$, with ϵ_0 very close to zero. In our simulations we find a bistable region [12] for small D that shrinks and disappears for $D > 2$, see Fig.(2(e)),

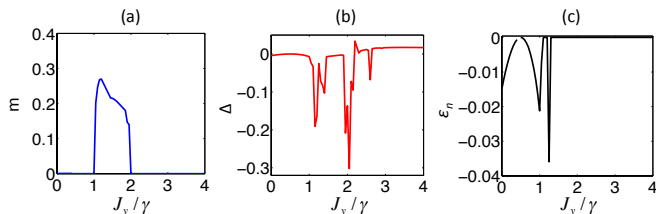


FIG. 4: **Ferromagnetic order parameter and error measures.** This is computed for the XYZ model, for $J_x = 0.5$, $J_z = 1$ and $D = 4$, with the order parameter as an average of $|M_x| = |\langle \sigma_x \rangle|$ over the two sites a and b in our 2D PEPO construction of ρ , i.e., $m \equiv (|M_x^a| + |M_x^b|)/2$. In (a) we observe no re-entrance of the ferromagnetic order m at large values of J_y/γ . In (b) we show $\Delta \equiv \# \langle \rho_s | \mathcal{L}_\# | \rho_s \rangle \#$, and in (c) we show $\epsilon_n \equiv \sum_{i|\nu_i < 0} \nu_i(\rho_n)$ for $n = 4$ contiguous spins in a 2×2 plaquette. Larger errors as quantified by Δ and ϵ_n appear around the phase transitions. Larger bond dimensions did not change the conclusion.

therefore being a unique steady state for large bond dimension. In Fig.(2(f)) we show the evolution of the 4-site operator-entanglement entropy throughout the algorithm for increasing values of γ . The stronger the dissipation, the weaker the operator entropy (which never exceeds the support of the PEPO), and therefore the better the performance of the algorithm, as claimed.

Next, we introduce non-zero values of the parallel field h_z . In some regions of the phase diagram, mean-field and correlated state variational methods predict the existence of an “antiferromagnetic” (AF) phase, where n_\uparrow attains different values between nearest-neighbours in the square lattice [11]. In our simulations we have also found this antiferromagnetic region up to $D = 5$, see Fig.(3) for $V = 5\gamma$, $\gamma = 0.1$, where for comparison we also show the data from Ref.[11] for the variational ansatz with product states (the correlated ansatz produced the a decrease in AF ordering upon including correlations, which is consistent with the disappearance of the AF phase for large bond dimensions). Quite surprisingly, however, we find no AF phase for $D = 6, 7, 8$ and 9 around this region. The AF phase thus disappears for large bond dimensions and for these values of the parameters. Notice that, however, this does not rule out the possibility of an AF phase appearing at some other parameter region.

Additionally, we have simulated a dissipative spin-1/2 XYZ model on an infinite 2D square lattice, with Hamiltonian $H = \sum_{\langle i,j \rangle} (J_x \sigma_x^{[i]} \sigma_x^{[j]} + J_y \sigma_y^{[i]} \sigma_y^{[j]} + J_z \sigma_z^{[i]} \sigma_z^{[j]})$, and the same jump operators $L_\mu = \sqrt{\gamma} \sigma_-^{[\mu]}$. This model has been analyzed recently by cluster mean-field and corner space renormalization methods [10, 13]. In particular, in Ref.[10], a possible re-entrance of the ferromagnetic phase at large coupling was discussed. In our simulations at large bond dimension we found no signal of such an effect, see Fig.(4) for results in the regime $J_x = 0.5$, $J_z = 1$, and $D = 4$. Even larger bond dimensions did not change this,

in agreement with the asymptotic conclusion of Ref.[10].

DISCUSSION

Here we presented a simple TN method to approximate steady states for 2D quantum lattice systems of infinite size. Our approach relies on the hypothesis that when the dissipative fixed-point attractor is strong, then it drives the simulation to a good approximation of the steady state. We benchmarked our method with dissipative Ising and XYZ models. Future applications include the engineering of topologically-ordered states by dissipation in 2D quantum lattice systems. It could also be applied to finite-temperature states, provided that a microscopic model for the coupling to the heat bath is included. Finally, it would be interesting to understand these results in the context of area-laws for rapidly mixing dissipative quantum systems [62, 63].

METHODS

We used several tensor network methods in this paper. Summarizing, we used PEPOs to represent mixed states, simple update for the real-time evolution, and corner transfer matrices to compute local observables in the thermodynamic limit. We also computed the operator-entanglement entropy using such methods, and by additionally simplifying the calculation of the eigenvalues of the reduced density matrix of a block using the tensors obtained from the simple update. A detailed explanation can be found in the Supplementary Information.

Data availability: all relevant data in this paper are available from the authors.

Code availability: all numerical codes in this paper are available upon request to the authors.

Acknowledgements: A. K. and R. O. acknowledge JGU, DFG GZ OR 381/1-1, DFG GZ OR 381/3-1, and discussions with I. McCulloch, A. Gangat, Y.-Jer Kao, M. Rizzi, D. Porrás, J. Eisert, J. J. García-Ripoll, and C. Ciuti. H. W. acknowledges the Volkswagen Foundation, DFG SFB 1227 (DQ-mat) and SPP 1929 (GiRyd).

Authors contribution: all authors contributed to all aspects of this work

Competing financial interests: this research has no competing financial interests.

* Electronic address: roman.orus@uni-mainz.de

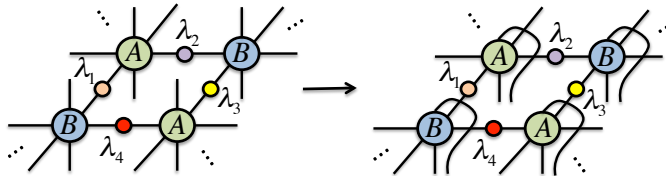
[1] M. Schlosshauer, “Decoherence, the measurement problem, and interpretations of quantum mechanics”, Rev. Mod. Phys. **76** 1267 (2005).

- [2] S. Vinjanampathy and J. Anders, “Quantum Thermodynamics”, *Con. Phys.* **57**, 3, 1-35 (2016).
- [3] S. Diehl *et al*, “Topology by dissipation in atomic quantum wires”, *Nat. Phys.* **7**, 971-977 (2011).
- [4] F. Verstraete, M. M. Wolf and J. I. Cirac, “Quantum computation and quantum-state engineering driven by dissipation”, *Nat. Phys.* **5**, 633-636 (2009).
- [5] M. Hönig *et al*, “Steady-state crystallization of Rydberg excitations in an optically driven lattice gas”, *Phys. Rev. A* **87**, 023401 (2013).
- [6] I. Pizorn, “Bose Hubbard model far from equilibrium”, *Phys. Rev. A* **88**, 043635 (2013).
- [7] F. W. G. Transchel, A. Milsted and T. Osborne, “A Monte Carlo Time-Dependent Variational Principle”, preprint at <http://arxiv.org/abs/1411.5546> (2014).
- [8] A. H. Werner *et al*, “A positive tensor network approach for simulating open quantum many-body systems”, *Phys. Rev. Lett.* **116**, 237201 (2016).
- [9] F. Iemini *et al*, “Dissipative topological superconductors in number-conserving systems”, *Phys. Rev. B* **93**, 115113 (2016).
- [10] J. Jin *et al*, “Cluster Mean-Field Approach to the Steady-State Phase Diagram of Dissipative Spin Systems”, *Phys. Rev. X* **6**, 031011 (2016).
- [11] H. Weimer, “Variational analysis of driven-dissipative Rydberg gases”, *Phys. Rev. A* **91**, 063401 (2015).
- [12] H. Weimer, “Variational principle for steady states of dissipative quantum many-body systems”, *Phys. Rev. Lett.* **114**, 040402 (2015).
- [13] R. Rota *et al*, “Critical behavior of dissipative two-dimensional spin lattices”, *Phys. Rev. B* **95**, 134431 (2017).
- [14] R. Orús, “A Practical Introduction to Tensor Networks: Matrix Product States and Projected Entangled Pair States”, *Annals of Physics* **349** 117-158 (2014).
- [15] J. Eisert, “Entanglement and tensor network states”, *Modelling and Sim.* **3**, 520 (2013).
- [16] N. Schuch, “Condensed Matter Applications of Entanglement Theory”, QIP, Lecture Notes of the 44th IFF Spring School (2013).
- [17] J. I Cirac and F. Verstraete, “Renormalization and tensor product states in spin chains and lattices”, *J. Phys. A: Math. Theor.* **42**, 504004 (2009)
- [18] F. Verstraete, J. I. Cirac and V. Murg, “Matrix Product States, Projected Entangled Pair States, and variational renormalization group methods for quantum spin systems”, *Adv. Phys.* **57**, 143 (2008).
- [19] E. Mascarenhas, H. Flayac, and V. Savona, “Matrix-product-operator approach to the nonequilibrium steady state of driven-dissipative quantum arrays”, *Phys. Rev. A* **92**, 022116 (2015).
- [20] J. Cui, J. I. Cirac, and M. C. Bañuls, “Variational Matrix Product Operators for the Steady State of Dissipative Quantum Systems”, *Phys. Rev. Lett.* **114**, 220601 (2015).
- [21] J. J. Mendoza-Arenas *et al*, “Beyond mean-field bistability in driven-dissipative lattices: bunching-antibunching transition and quantum simulation” *Phys. Rev. A* **93**, 023821 (2016).
- [22] P. Czarnik and J. Dziarmaga, “Variational Approach to Projected Entangled Pair States at Finite Temperature”, *Phys. Rev. B* **92**, 035152 (2015).
- [23] P. Czarnik, M. M. Rams and J. Dziarmaga, “Variational tensor network renormalization in imaginary time: benchmark results in the Hubbard model at finite temperature”, *Phys. Rev. B* **94**, 235142 (2016).
- [24] M. Zwolak and G. Vidal, “Mixed-state dynamics in one-dimensional quantum lattice systems: a time-dependent superoperator renormalization algorithm”, *Phys. Rev. Lett.* **93**, 207205 (2004).
- [25] I. P. McCulloch, “Infinite size density matrix renormalization group, revisited”, preprint at <http://arxiv.org/abs/0804.2509> (2008).
- [26] G. Vidal, “Efficient classical simulation of slightly entangled quantum computations”, *Phys. Rev. Lett.* **91**, 147902 (2003).
- [27] G. Vidal, “Efficient simulation of one-dimensional quantum many-body systems”, *Phys. Rev. Lett.* **93**, 040502 (2004).
- [28] G. de las Cuevas *et al*, “Purifications of multipartite states: limitations and constructive methods”, *New J. Phys.* **15**, 123021 (2013).
- [29] F. Verstraete and J. I. Cirac, “Renormalization algorithms for Quantum-Many Body Systems in two and higher dimensions”, preprint at <https://arxiv.org/abs/cond-mat/0407066> (2004).
- [30] J. Jordan *et al*, *Phys. Rev. Lett.* **101**, 250602 (2008).
- [31] H. C. Jiang, Z. Y. Weng and T. Xiang, “Classical simulation of infinite-size quantum lattice systems in two spatial dimensions”, *Phys. Rev. Lett.* **101**, 090603 (2008).
- [32] R. J. Baxter, “Corner transfer matrix”, *Physica A* **106**, pp18-27 (1981).
- [33] R. J. Baxter, “Exactly Solved Models in Statistical Mechanics”, Academic Press, London, (1982).
- [34] R. J. Baxter, “Dimers on a rectangular lattice”, *J. Math. Phys.* **9**, 650 (1968).
- [35] R. J. Baxter, “Variational approximations for square lattice models in statistical mechanics”, *J. Stat. Phys.* **19** 461 (1978).
- [36] T. Nishino and K. Okunishi, “Corner Transfer Matrix Renormalization Group Methods”, *J. Phys. Soc. Jpn.* **65** pp. 891-894 (1996).
- [37] T. Nishino and K. Okunishi, “Corner Transfer Matrix Algorithm for Classical Renormalization Group”, *J. Phys. Soc. Jp.* **66**, 3040 (1997).
- [38] R. Orús and G. Vidal, “Simulation of two dimensional quantum systems on an infinite lattice revisited: corner transfer matrix for tensor contraction”, *Phys. Rev. B* **80**, 094403 (2009).
- [39] R. Orús, “Exploring corner transfer matrices and corner tensors for the classical simulation of quantum lattice systems”, *Phys. Rev. B* **85**, 205117 (2012).
- [40] Ho N. Phien *et al*, “Infinite projected entangled pair states algorithm improved: Fast full update and gauge fixing”, *Phys. Rev. B* **92**, 035142 (2015).
- [41] L. Vanderstraeten, *et al*, “Gradient methods for variational optimization of projected entangled-pair states”, *Phys. Rev. B* **94**, 155123 (2016).
- [42] P. Corboz, “Variational optimization with infinite projected entangled-pair states”, *Phys. Rev. B* **94**, 035133 (2016).
- [43] M. Levin, and C. P. Nave, “Tensor Renormalization Group Approach to Two-Dimensional Classical Lattice Models”, *Phys. Rev. Lett.* **99**, 120601 (2007).
- [44] Z. Y. Xie *et al*, “Second Renormalization of Tensor-Network States”, *Phys. Rev. Lett.* **103**, 160601 (2009).
- [45] H. H. Zhao *et al*, “Renormalization of tensor-network states”, *Phys. Rev. B* **81**, 174411 (2010).

- [46] Z. Y. Xie *et al*, “Coarse-graining renormalization by higher-order singular value decomposition”, *Phys. Rev. B* **86**, 045139 (2012).
- [47] G. Evenbly and G. Vidal, “Tensor Network Renormalization”, *Phys. Rev. Lett.* **115**, 180405 (2015).
- [48] G. Vidal, “Classical simulation of infinite-size quantum lattice systems in one spatial dimension”, *Phys. Rev. Lett.* **98**, 070201 (2007).
- [49] R. Orús and G. Vidal, “Infinite time-evolving block decimation algorithm beyond unitary evolution”, *Phys. Rev. B* **78**, 155117 (2008).
- [50] A. A. Gangat, T. I and Y.-Jer Kao, “Steady States of Infinite-Size Dissipative Quantum Chains via Imaginary Time Evolution”, *Phys. Rev. Lett.* **119**, 010501 (2017).
- [51] S. R. White, “Density matrix formulation for quantum renormalization groups”, *Phys. Rev. Lett.* **69**, 28632866 (1992).
- [52] S. R. White, “Density-matrix algorithms for quantum renormalization groups”, *Phys. Rev. B* **48**, 10345 (1992).
- [53] U. Schollwöck, “The density-matrix renormalization group”, *Rev. Mod. Phys.* **77**, 259 (2005).
- [54] U. Schollwöck, “The density-matrix renormalization group in the age of matrix product states”, *Annals of Physics* **326**, 96 (2011).
- [55] F. Letscher *et al*, “Bistability vs. Metastability in Driven Dissipative Rydberg Gases”, preprint at <https://arxiv.org/abs/1611.00627> (2016).
- [56] N. Malossi *et al*, “Full Counting Statistics and Phase Diagram of a Dissipative Rydberg Gas”, *Phys. Rev. Lett.* **113**, 023006 (2014).
- [57] Tony E. Lee, H. Häfner and M. C. Cross, “Antiferromagnetic phase transition in a nonequilibrium lattice of Rydberg atoms”, *Phys. Rev. A* **84**, 031402 (2011).
- [58] M. Marcuzzi *et al*, “Universal non-equilibrium properties of dissipative Rydberg gases”, *Phys. Rev. Lett.* **113**, 210401 (2014).
- [59] M. F. Maghrebi and A. V. Gorshkov, “Nonequilibrium many-body steady states via Keldysh formalism”, *Phys. Rev. B* **93**, 014307 (2016).
- [60] M. Hönig *et al*, “Antiferromagnetic long-range order in dissipative Rydberg lattices”, *Phys. Rev. A* **90**, 021603 (2014).
- [61] M. Hönig *et al*, “Steady-state crystallization of Rydberg excitations in an optically driven lattice gas”, *Phys. Rev. A* **87**, 023401 (2013).
- [62] A. Lucia *et al*, “Rapid mixing and stability of quantum dissipative systems”, *Phys. Rev. A* **91**, 040302 (2015).
- [63] F. G. S. L. Brandao *et al*, “Area law for fixed points of rapidly mixing dissipative quantum systems”, *J. Math. Phys.* **56**, 102202 (2015).

Supplementary Note 1: Projected Entangled-Pair Operators

Projected Entangled-Pair Operators (PEPO) are simply the operator version of Projected Entangled-Pair States (PEPS), in the same way that Matrix Product Operator (MPO) are the operator version of Matrix Product States (MPS) for the $1D$ case [1–5]. More specifically, a $2D$ PEPO is an operator that acts on a $2D$ PEPS and produces a new PEPS, and admits a tensor network description as in Supplementary Fig.(1). In principle there is no restriction on the coefficients of the tensors, so that PEPOs can represent, at least a priori, operators of any kind: generic, unitary, positive, and so on. In our case we use PEPOs to describe reduced density matrices, which are positive by construction. However, a PEPO does not need to be necessarily positive, and therefore the negative eigenvalues need to be under control in order to produce an accurate representation of a physical mixed state, as explained in the main text. Moreover, one can “vectorize” the PEPO, so that the resulting object can be treated as a $2D$ PEPS with double physical indices. Importantly, in this supplementary material we add diagonal weight matrices λ at the links. This is convenient in order to implement the so-called simple update, which we comment in the next section. In practice we also used a 2-site unit cell with tensors A and B at every site, and diagonal positive matrices $\lambda_1, \lambda_2, \lambda_3$ and λ_4 at every link, as shown in Supplementary Fig.(1).



SUPPLEMENTARY FIG. 1: **From operator to vector.** PEPO on an infinite $2D$ lattice, with a 2-site unit cell, tensors A and B at sites, and $\lambda_1, \lambda_2, \lambda_3$ and λ_4 at the links, as well as its vectorization.

Supplementary Note 2: Simple update

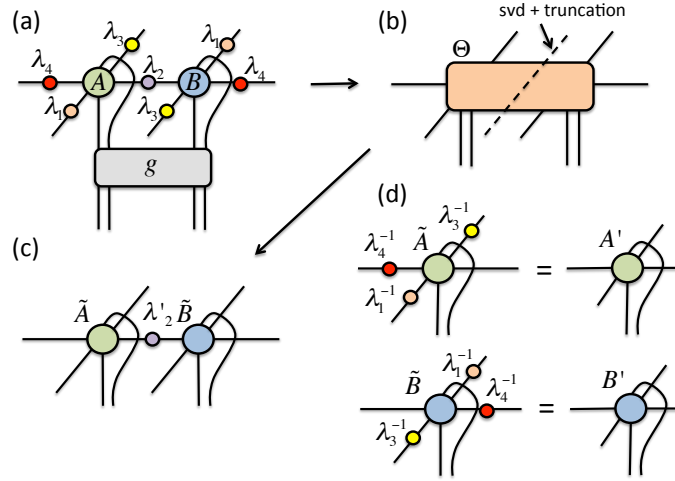
The time evolution generated by the Liouvillian superoperator is broken via a Trotter decomposition into small two-body gates, namely

$$e^{T\mathcal{L}_\#} = (e^{\delta t\mathcal{L}_\#})^{T/\delta t} \approx \left(\prod_{\langle i,j \rangle} e^{\delta t\mathcal{L}_\#^{[i,j]}} \right)^{T/\delta t} \equiv \left(\prod_{\langle i,j \rangle} g^{[i,j]} \right)^{T/\delta t}, \quad (3)$$

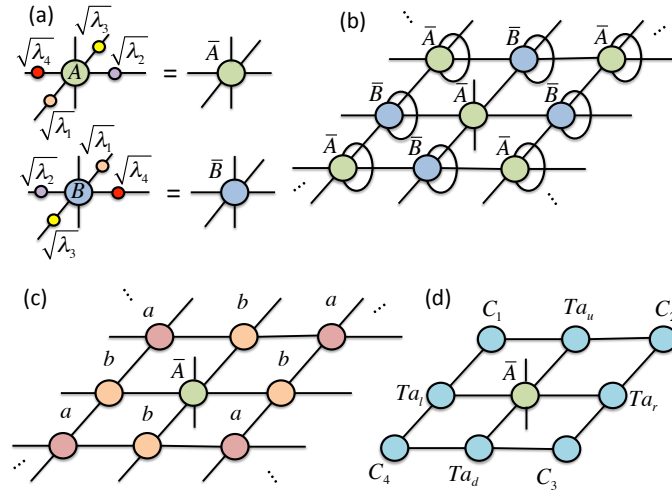
where we implemented for concreteness the first-order Trotter approximation, and we defined the 2-body gates $g^{[i,j]}$ acting on the different links. The action of one of these gates in a given link is accounted for by defining new approximated PEPO tensors following the scheme in Supplementary Fig.(2), called *simple update* [1–5]. This is the direct generalization of the update rule of the TEBD algorithm for $1D$ MPS [6, 7]. The update is locally optimal in $1D$, whereas only approximate in $2D$ because it does not take into account the effect of the environment of the link in the approximation of the tensors. Still, it is remarkably efficient, and produces good results for gapped phases with small correlation length.

Supplementary Note 3: Local observables

The calculation of local observables follows from an approximate contraction of the $2D$ tensor network using corner transfer matrices (CTM) [8–15]. For instance, the calculation of the (unnormalized) 1-site density matrix is done as shown in Supplementary Fig.(3). First, square-roots of the λ tensors are contracted with the tensors at every site as in Supplementary Fig.(3(a)). The partial trace is taken as in Supplementary Fig.(3(b)), which produces a tensor network as in Supplementary Fig.(3(c)). This tensor network is approximated using four CTMs C_1, C_2, C_3 and C_4 , as well as four half-row/column transfer matrices Ta_u, Ta_r, Ta_d and Ta_l as in Supplementary Fig.(3(d)) – which would be eight for a 4-site unit cell –. These approximating tensors are the *effective environment* of the site where we compute the reduced density matrix.



SUPPLEMENTARY FIG. 2: **Tensor update with the simple update.** A 2-body gate g acts on a given link of the PEPO as in (a), and the contraction produces tensor Θ as in (b). This tensor is broken into two pieces by a singular value decomposition (svd), and after truncation of the singular values in D (by keeping the D largest ones) it produces the structure in (c). The new tensor λ'_2 corresponds to the truncated singular values. The new tensors A' and B' at the sites are computed as in (d).



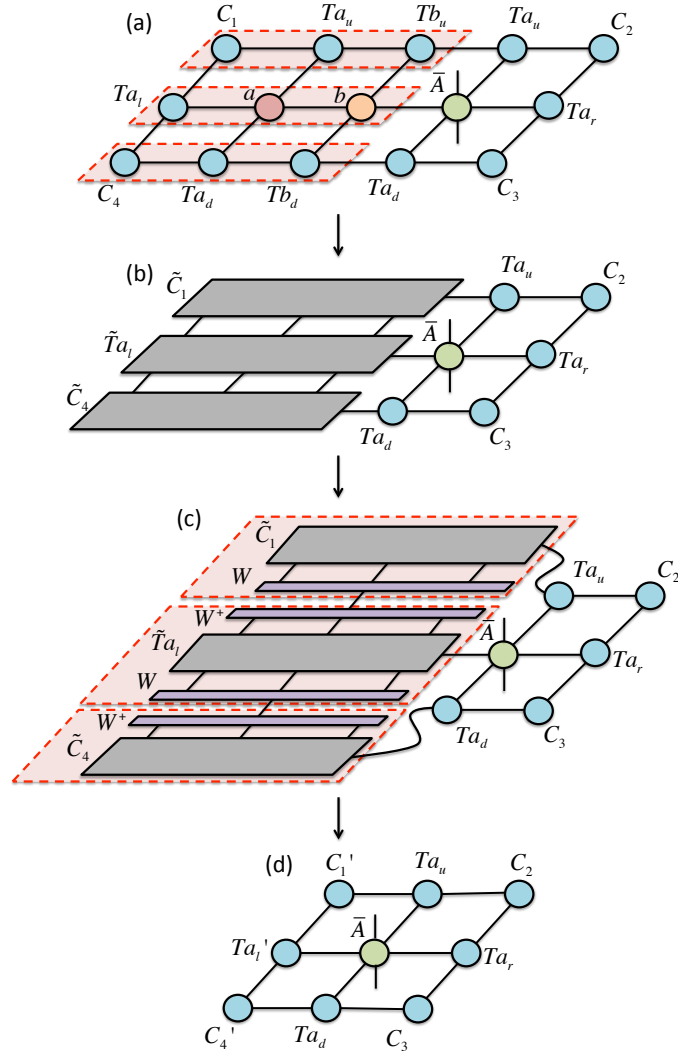
SUPPLEMENTARY FIG. 3: **Computing a 1-site reduced density matrix.** (a) Square roots of the λ tensors at the links are contracted with the tensors at the sites, in order to have a tensor network with one tensor per site; (b) partial trace over the environment of one site in the lattice; (c) tensor network obtained as a result of the partial trace; (d) approximation of the contraction in (c) in terms of CTMs and half row/column tensors.

In Supplementary Fig.(4) we provide the basic details of how the tensors for the effective environment are computed [8–15]. In particular, for a “left move”, two rows are inserted in the network and absorbed towards the left. The growth of the bond index is renormalized by an isometry W (see Supplementary Fig.(4(c)), which can be computed according to several prescriptions [8–15]. The procedure follows by iterating directional moves along the left, right, up and down directions until convergence.

Supplementary Note 4: Operator-entanglement entropy

We define the operator-entanglement entropy as

$$S_{\text{op}}(\rho) \equiv -\text{tr}(\sigma_{\#} \log_2 \sigma_{\#}), \quad (4)$$



SUPPLEMENTARY FIG. 4: **Left move of the iterative procedure to compute the approximate environment.** We follow the step in Ref.[13]. (a) Two columns are inserted; (b) new exact left tensors are defined; (c) renormalization of the bond indices by an isometry W ; (d) new renormalized environment tensors on the left.

with

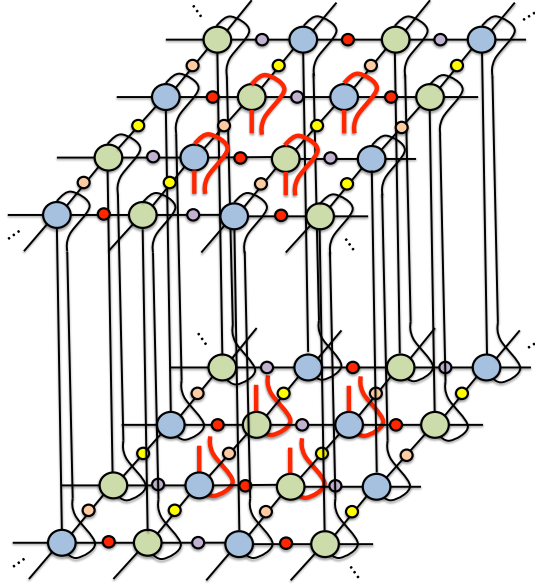
$$\sigma_{\sharp} \equiv \text{tr}_E (|\rho\rangle_{\sharp} \langle \rho|). \quad (5)$$

In the above equations, $|\rho\rangle_{\sharp}$ is the vectorized reduced density matrix, and tr_E is the partial trace over the sites for which we wish to compute the entropy. In a nutshell: this is the entanglement entropy of $|\rho\rangle_{\sharp}$, the vectorized density matrix, understood as a pure state. As such, this is *not* a measure of entanglement of the mixed state ρ . However, this is the relevant measure of correlations for our purposes, since it is upper-bounded directly by the bond dimension of the PEPO. Namely, if the PEPO has bond dimension D , then for a block of $L \times L$ sites one has

$$S_{\text{op}}(\rho) \leq 4L \log_2 D, \quad (6)$$

which means that we can use it to quantify how large needs to be our bond dimension D for the PEPO, being this directly connected to the computational cost and the accuracy of the method [16].

In what follows we explain to procedures to compute $S_{\text{op}}(\rho)$: one fully taking into account the environment of the block, and one approximate taking into account some of the properties of the simple update.



SUPPLEMENTARY FIG. 5: **Full calculation of operator entanglement entropy.** Tensor network for the operator σ_{\sharp} , obtained after tracing out the degrees of freedom of the environment of a 2×2 block in the vector $|\rho\rangle_{\sharp}$. We omit the name of the tensors for clarity of the diagram. Open indices of σ_{\sharp} are shown in red.

Full calculation

The calculation taking into account the full environment follows the tensor contraction from Supplementary Fig.(5). In this case, we compute σ_{\sharp} by tracing out the degrees of freedom outside the block, as shown in the figure. The corresponding contraction can be approximated in the thermodynamic limit using the CTM method explained above.

Simple calculation

For the case of a phase with small correlation length, and using the information obtained from the simple update (namely, tensors at the sites and at the links), it is indeed possible to approximate, up to a good accuracy, the tensor network in Supplementary Fig.(5) by the one in Supplementary Fig.(6). In this approximation, one does not take the surrounding environment of the block fully into account. Instead, the effect of the environment is replaced by the effect of the λ tensors surrounding the block, which amounts to a mean-field approximation of the effective environment. Moreover, one can see that in such a case the eigenvalues of σ_{\sharp} can be approximated with good accuracy by the product of the squares of the surrounding λ tensors, i.e.,

$$\text{eig}(\sigma_{\sharp}) \approx \prod_{i \in \text{boundary}} (\lambda^{[i]})^2, \quad (7)$$

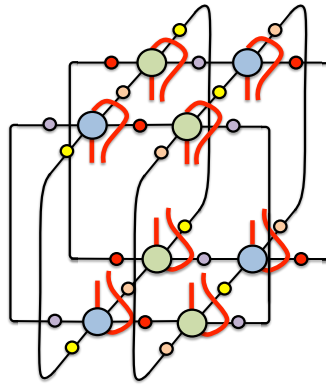
and therefore the operator entanglement entropy reads

$$S_{\text{op}}(\rho) \approx \sum_{i \in \text{boundary}} S_{\text{op}}^{[i]} \quad (8)$$

with

$$S_{\text{op}}^{[i]} \equiv - \sum_{\alpha=1}^D (\lambda_{\alpha}^{[i]})^2 \log_2 (\lambda_{\alpha}^{[i]})^2. \quad (9)$$

This approximation works very well in gapped phases computed via the simple update, and it is the one that we used in the main text.



SUPPLEMENTARY FIG. 6: **Simple calculation of operator entanglement entropy.** Tensor network for the operator σ_{μ} for a 2×2 block in the vector $|\rho\rangle_{\mu}$, with a mean-field approximation of the effective environment. We omit the name of the tensors for clarity of the diagram. Open indices of σ_{μ} are shown in red.

Supplementary References

* Electronic address: roman.orus@uni-mainz.de

- [1] R. Orús, “A Practical Introduction to Tensor Networks: Matrix Product States and Projected Entangled Pair States”, *Annals of Physics* **349** 117-158 (2014).
- [2] J. Eisert, “Entanglement and tensor network states”, *Modelling and Sim.* **3**, 520 (2013).
- [3] N. Schuch, “Condensed Matter Applications of Entanglement Theory”, QIP, Lecture Notes of the 44th IFF Spring School (2013).
- [4] J. I Cirac and F. Verstraete, “Renormalization and tensor product states in spin chains and lattices”, *J. Phys. A: Math. Theor.* **42**, 504004 (2009)
- [5] F. Verstraete, J. I. Cirac and V. Murg, “Matrix Product States, Projected Entangled Pair States, and variational renormalization group methods for quantum spin systems”, *Adv. Phys.* **57**, 143 (2008).
- [6] G. Vidal, “Efficient classical simulation of slightly entangled quantum computations”, *Phys. Rev. Lett.* **91**, 147902 (2003).
- [7] G. Vidal, “Efficient simulation of one-dimensional quantum many-body systems”, *Phys. Rev. Lett.* **93**, 040502 (2004).
- [8] R. J. Baxter, “Corner transfer matrix”, *Physica A* **106**, pp18-27 (1981).
- [9] R. J. Baxter, “Exactly Solved Models in Statistical Mechanics”, Academic Press, London, (1982).
- [10] R. J. Baxter, “Dimers on a rectangular lattice”, *J. Math. Phys.* **9**, 650 (1968).
- [11] R. J. Baxter, “Variational approximations for square lattice models in statistical mechanics”, *J. Stat. Phys.* **19** 461 (1978).
- [12] T. Nishino and K. Okunishi, “Corner Transfer Matrix Renormalization Group Methods”, *J. Phys. Soc. Jpn.* **65** pp. 891-894 (1996).
- [13] T. Nishino and K. Okunishi, “Corner Transfer Matrix Algorithm for Classical Renormalization Group”, *J. Phys. Soc. Jp.* **66**, 3040 (1997).
- [14] R. Orús and G. Vidal, “Simulation of two dimensional quantum systems on an infinite lattice revisited: corner transfer matrix for tensor contraction”, *Phys. Rev. B* **80**, 094403 (2009).
- [15] R. Orús, “Exploring corner transfer matrices and corner tensors for the classical simulation of quantum lattice systems”, *Phys. Rev. B* **85**, 205117 (2012).
- [16] S. Sahin, R. Orús, K. P. Schmidt, “Entanglement Continuous Unitary Transformations”, *Europhysics Letters* **117**, 20002 (2017).